Ocean Systems Engineering, Vol. 1, No. 1 (2011) 17-29
DOI: http://dx.doi.org/10.12989/ose.2011.1.1.017

Modeling of air cushion vehicle's flexible seals under steady state conditions

Steven F. Zalek*, Dale G. Karr[a], Sara Jabbarizadeh[b] and Kevin J. Maki[c]

Department of Naval Architecture and Marine Engineering, University of Michigan, USA
(Received July 26, 2010, Accepted February 10, 2011)

Abstract. The purpose of this paper is to demonstrate the efficacy of modeling a surface effect ship's air-cushion flexible seal utilizing a two-dimensional beam under steady state conditions. This effort is the initial phase of developing a more complex three-dimensional model of the air-seal-water fluid-structure interaction. The beam model incorporates the seal flexural rigidity and mass with large deformations while assuming linear elastic material response. The hydrodynamic pressure is derived utilizing the OpenFOAM computational fluid dynamic (CFD) solver for a given set of steady-state flow condition. The pressure distribution derived by the CFD solver is compared with the pressure required to deform the seal beam model. The air pressure, flow conditions and seal geometry are obtained from experimental analysis. The experimental data was derived from large-scale experimental tests utilizing a test apparatus of a canonical surface effect ship's flexible seal in a towing tank over a variety of test conditions.

Keywords: fluid structure interaction; beam; membrane; surface effect ship.

1. Experimental effort

1.1 Introduction

There is a demonstrated need for improved physics-based numerical modeling tools to adequately determine the expected performance of air cushion-supported vessels under the complex array of US naval vessel design environments. To improve these numerical tools, detailed physical behavior and characteristics of the seals are required. Surface-effect-ship (SES) seal experimental analysis has been conducted at US Naval facilities by Bresch (1976) and Wilson *et al*. (1979). The focus of their work was primarily on deriving the SES's global resistance characteristics. Malakoff and Davis (1981) investigated the SES finger-type seal performance in detail from a vibration and material longevity perspective. However, it appears that the physical data required for developing and validating adequate numerical models of SES bow seals is generally not available in the public domain.

A seal test apparatus was designed and constructed at the University of Michigan and operated at its towing tank facility to derive data and develop the requisite experimental methods. The local effort at the University of Michigan is part of a larger experimental program, with the following goals:

*Corresponding author, Ph.D., E-mail: zaleksf@umich.edu
[a]Professor
[b]Ph.D. Student
[c]Assistant Reserch Scientist

1. to devise and execute a large-scale, high Reynolds number SES bow seal fluid-structure physical experiment
2. to obtain a better understanding of the seal-air-cushion-water interface fundamental physics through a parameter matrix of experimental conditions
3. to obtain useful data for the development of physics-based numerical models

A relatively large SES seal test apparatus is utilized in order to minimize scale effects. The upper limit of the test apparatus size is constrained by the size and capabilities of the various experimental facilities at which it is used. The test apparatus primary structure is 12 feet long by 4 feet high by 5 feet wide with externally mounted structure and equipment increasing the overall size somewhat, as shown in Figs. 1 and 2.

It is important to note that the seal test apparatus is not intended to model any particular type of SES vessel; it is intended to provide a platform for investigating SES seal fluid-structure interaction. Numerical modelers are expected to utilize this data to model the experiment in order to validate their code performance.

The test apparatus is designed for relatively high flow conditions aligned in the longitudinal (x) direction and has the ability to withstand large transient hydrodynamic loads. It is primarily designed for testing seal resistance in both calm water conditions and with small amplitude waves. The test apparatus is also currently being analyzed for use in dynamic conditions where seal

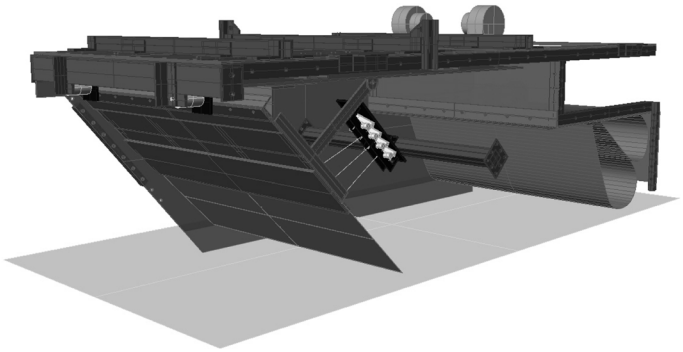

Fig. 1 Bow-quarter cut-away view of the test apparatus (rendering) configured with the flat-membrane seal

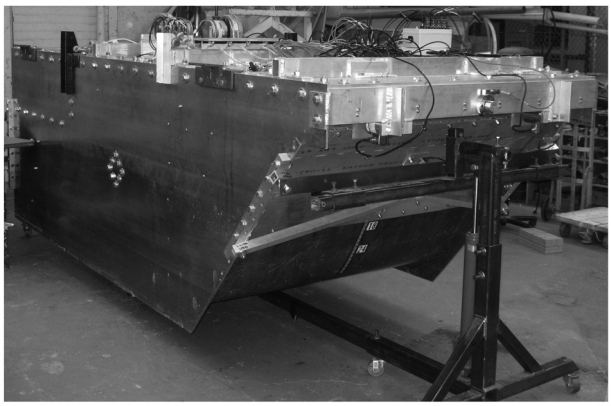

Fig. 2 Seal test apparatus located in the fabrication shop

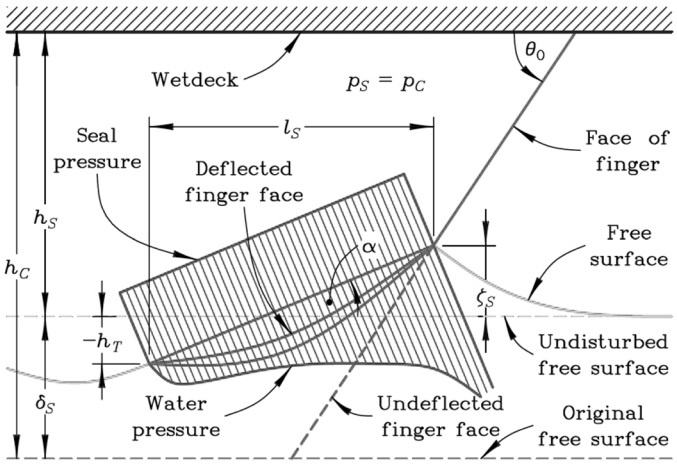

Fig. 3 SES bow seal theoretical model geometry and parameters (Doctors and McKesson 2006)

behavior and cushion dynamics would be investigated under forced motion conditions.

Figs. 1 and 2 show the test apparatus configured with a flat-membrane type seal, which was proposed for the Rohr Marine, Inc., 3KSES vessel during the 1980s. Modern SES craft utilize flnger-type seal, which provides an overall better sealing system stability in a dynamic environment (Graham and Sullivan 2002). The simpler geometry of the flat-membrane seal provides more favorable conditions for identifying and quantifying the fundamental physics of the seal fluid-structure interaction and comparing the results to two-dimensional seal numerical models. However, it is a greater challenge to maintain an adequate air cushion seal under all desirable test conditions. Fig. 3 shows the two-dimensional theoretical seal model devised by Doctors and McKesson (2006), for which the test apparatus attempts to acquire supporting physical data.

1.2 Seal experiments

The primary goal of the test apparatus instrumentation suite is to obtain the seal total thrust (*x*-direction) force, mean geometric form and bow wave height for a given test apparatus speed, cushion pressure and seal initial immersion depth. The seal monitoring system is outtted with load cells, pressure transducers, ultrasonic bow wave height sensor, digital video and oncontact position sensors in order to acquire these data.

The black flexible membrane seal is marked with a white 3 inch × 3 inch grid to allow digital optical analysis. The star-board side of the test apparatus is also marked with a 1 inch × 1 inch black and white checkerboard grid to allow digital optical analysis of the seal edge, as shown in Fig. 4. Two digital video cameras are mounted on the port side of the cushion cavity above the seal and arranged to capture the seal deflection and free surface profile aft until it encounters the stern seal. Four 2 psig pressure transducer (0.15% full scale repeatability) sensor points are located on the cushion-side of the bow seal plate.

Two 500 pound load cells (0.05% full scale repeatability) couple the bow seal mounting plate, which is suspended by the rails and linear bearings, to the thrust plate, which is anchored to the test apparatus frame. These load cells capture the total thrust force on the seal due to the cushion air pressure, and air resistance and water resistance due to forward motion.

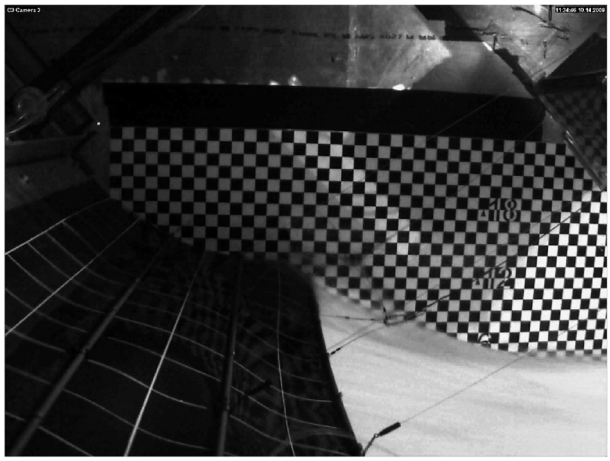

Fig. 4 Transverse view of the bow seal test conditions: forward speed 8 ft/sec, cushion pressure of 4.24 inches H_2O (0.153 psig) and 9.0 inches seal initial immersion depth

The instrument data as well as carriage forward speed is collected with a National Instruments data collection system. The video data is collected with a separate digital video system and correlated with the instrument data with a timing signal. Fig. 4 shows an interior view of the bow seal with the following experimental condition: forward speed 8 ft/sec, cushion pressure of 4.24 inches H_2O (0.153 psig) and 9.0 inches seal initial immersion depth with a total calculated hydrodynamic thrust force of approximately 124 lb.

The bow seal is mounted to a plate that isolates motion to the longitudinal (x) direction. The upper portion of the bow seal is stiffened aluminum plate mounted at a 45 degree angle to the water plane and main deck. This upper seal plate spans the entire width of the cushion cavity with the exception of approximately 1/16 inch gap on either side, which is covered by a low-friction seal to minimize cushion air loss. The lower portion of the seal is a flexible membrane fabricated from 1/8 inch thick vulcanized neoprene rubber with two nylon mesh inserts devised to minimize stretching. The membrane seal is trimmed to fit very closely to the test apparatus side walls to minimize cushion air loss. The seal is fitted with three transverse stiffeners to help maintain a full transverse profile in the event of three-dimensional effects as shown in Fig. 4; the seal is free to flex about the transverse (y) axis. This flexible portion of the seal is also fitted with light-weight restraint wires that prevent it from extending forward of a 45 degree line made with the main deck when subject to a high static cushion pressure.

These experiments did not utilize a mechanism for directly determining the local flow fleld physics: velocity and pressure. The specific flow fleld physics was of secondary concern to developing the experimental procedures for this series of experiments. Hence, the net pressure on the seal is derived through numerical methods, as discussed in the subsequent sections.

1.3 Experiment results

The experiment data collected includes forward speed, cushion air pressure, seal position and

motion and total thrust load on the seal. For a given test run the data is statistically averaged over the interval when the data indicates the system conditions are quasi-steady (i.e., unchanging time-averaged forward speed and cushion pressure).

The hydrodynamic resistance, Eq. (1), due to the seal dragging in the water is derived from the the balance of forces on the seal system: total load cell force $F_{loadcell}$, hydrodynamic resistance F_{hydro} due to the seal contact with the water, air resistance F_{air} and air cushion force $F_{cushion}$.

$$F_{hydro} = F_{loadcell} - F_{cushion} - F_{air} \tag{1}$$

The on-contact sensors provide seal position at three points along the flexible seal center line from an instrument pair for each point, providing a distance and angle from the sensor mount. The seal point distance is provided by a high-accuracy, low-tension string potentiometer; the angle is provided by a high-accuracy rotary potentiometer. The seal position indicated by the on-contact sensor compares favorably with the position indicated by the seal edge next to the checkerboard grid. The impact of the on-contact sensor is minimal, generally contributing less than 0.9 lbs of thrust force which is less than 1-2% for most test conditions.

A summary of the experimental results, for steady state conditions are shown in the following Figs. 5(a) and 5(b). They are differentiated by initial seal immersion depth. Multiple test runs were

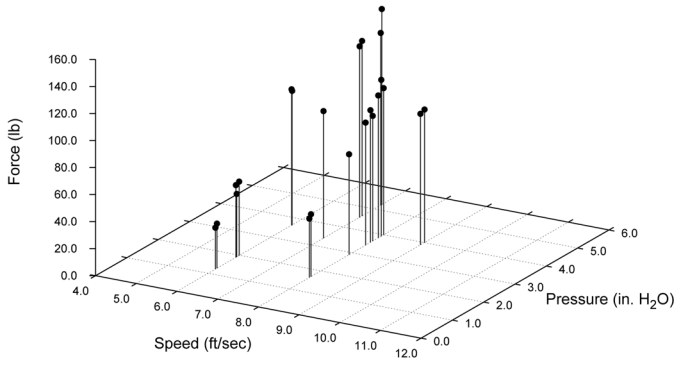

(a) 7.5 inch initial seal immersion

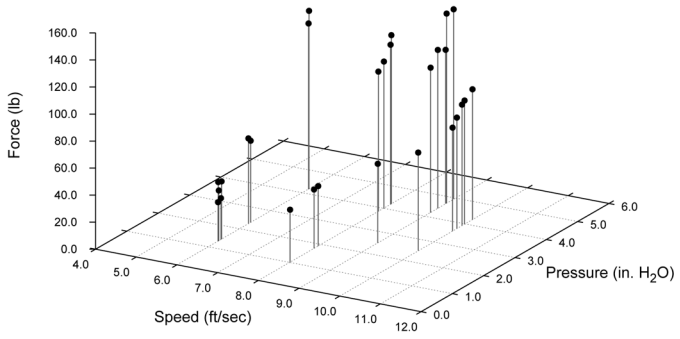

(b) 9.0 inch initial seal immersion

Fig. 5 Bow seal hydrodynamic force F_{hydro} with respect to forward speed and cushion air pressure

conducted at identical initial test conditions in order to investigate the repeatability of the results and acquire a statistically larger sample. The total hydrodynamic force on the seal generally increases with increased cushion pressure, seal initial immersion depth and forward speed. The steady state seal geometry along with the hydrodynamic force data is utilized for the CFD analysis and the seal numerical model.

2. CFD model

2.1 Problem formulation

The fluid stress that acts on the seal is predicted using a solver from the OpenFOAM open source CFD library. The numerical technique solves the unsteady equations for the conservation of mass and fluid momentum on a fluid grid using the flnite-volume method. The complex air-water interface is handled with the Volume-of-Fluid (VOF) method. The pressure variable is determined such that the flow fleld satisfies no divergence using a PISO algorithm. All discretizations are second-order accurate.

Two cases are studied under the assumption that the fluid domain is rigid, as shown in Table 1. The first approximation would be the seal acts upon the water like a flat plate. The flat-body planning problem has been well studied, and this simplified problem is chosen as the starting point for our present analysis. The second case that we simulate in this work is that of the experimentally measured shape of the SES seal. The physical experiment shows that the flow and structural response is indeed unsteady, but for our current analysis we use the time-averaged position of the seal in a standard operating condition (cushion pressure and forward speed).

2.2 Analysis results

The unsteady equations of motion are solved for sufficient time such that the pressure on the body is dominantly steady. In this case there is an oscillation of the stress on the body due to wave

Table 1 Conditions for CFD analysis

(a) Experimentally measured shape simulation		
Condition	Value	Units
Forward Speed	8.0	ft/sec
Seal Arc-length	19.3	inches
Cushion Air Pressure	0.153	psig
(b) Flat-plate simulation		
Condition	Value	Table
Forward Speed	9.0	ft/sec
Seal Arc-length	11.8	inches
Cushion Air Pressure	0.153	psig
Seal Angle-of-attack	17.6	degrees

(a) Free surface profile

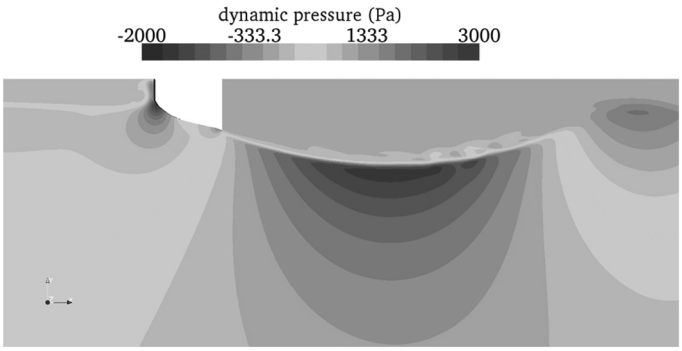

(b) Pressure distribution

Fig. 6 Fluid domain for experimental condition: forward speed 8 ft/sec, cushion pressure of 4.24 inches H_2O (0.153 psig) and 9.0 inches seal initial immersion depth

sloshing in flow domain. The time-averaged value of the stress in the fluid is used to eliminate this oscillation. Fig. 6(a) shows the free-surface profile in the fluid domain for the case where the body is that which was experimentally measured. In Fig. 6(b) the resulting pressure fleld is shown.

The pressure dominates the fluid stress on the boundary, and hence it is sufficient to examine solely this component in comparing the case of a flat planning plate to that of the experimentally measured shape. Fig. 7(a) shows the pressure profile along both the flat shape and that which was experimentally determined. The horizontal axis is non-dimensionalized using the total length of the seal. It is interesting to see that the magnitude of the pressure in both cases is similar. Since each case was executed at a different forward speed, it is instructive to examine the maximum as the fraction of dynamic pressure. This would result in the profiles that are plotted in Fig. 7(b). In this case the difference in forward speed of 1 ft/s does not alter the relative magnitude of the pressure flelds.

3. Bow seal numerical model

3.1 Scope of the Model

In the analysis of the seal deflection, we first selected a representative strip of the seal along the length of which the coordinates we determined from a photograph taken during transit. The seal strip was treated as a flexible elastic beam subjected to hydrodynamic pressure and opposing cushion pressure. Because the deflections are large, much larger than the thickness of the seal, large

displacements were presumed with the equilibrium established for a quasi-static, steady state configuration. Pressures were thus considered to act in a direction normal to the surface of the seal.

3.2 Mathematical foundation

In the displaced configuration, the surface tangent direction is determined by its angle of inclination with the horizontal, θ. The net transverse pressure q, is determined as the difference between the cushion and hydrodynamic pressures, as shown in Eq. (2)

$$q = p_{cushion} - p_{hydro} \tag{2}$$

The weight density of the seal itself is determined to be approximately $w_0 = 0.005$ lb/in^2. The shear force intensity, V, is considered to act in the direction normal to the displaced surface. Also, due to the large displacements the axial force intensity, T, is included; this yields upon summation of transverse forces acting on an element of arc length, ds, as shown in Eq. (3)

$$\frac{dV}{ds} = q + w_0 \cos\theta - T\frac{d\theta}{ds} \tag{3}$$

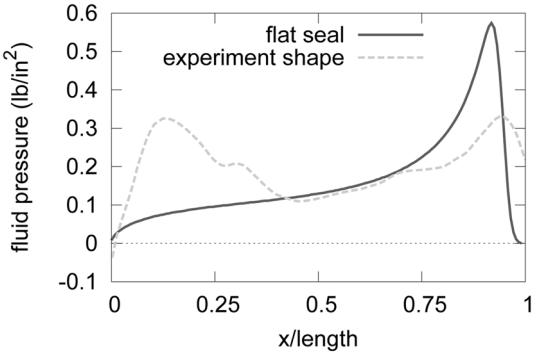

(a) Pressure magnitude vs nondimensionalized length

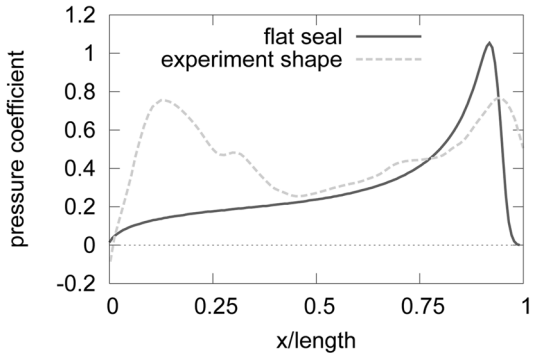

(b) Pressure coefficient vs nondimensionalized length

Fig. 7 Pressure profile along a flat plate shaped seal and that which was experimentally determined

The summation of tangential forces yields Eq. (4)

$$\frac{dT}{ds} = w_0 \sin\theta - V\frac{d\theta}{ds} \tag{4}$$

Consideration of the flexural rigidity of the cross section yields the well known Eq. 5, and summation of moments of the beam segments yields Eq. (6)

$$M = EI\frac{d\theta}{ds} \tag{5}$$

$$\frac{dM}{ds} = -V \tag{6}$$

Substituting Eqs. (5) and (6) into the equilibrium equations, Eqs. (3) and (4), yields the shear force and tension force intensities, Eqs. (7) and (8), respectively.

$$V = -EI\frac{d^2\theta}{ds^2} \tag{7}$$

$$T = \int\left[w_0 \sin\theta + EI\frac{d^2\theta}{ds^2}\frac{d\theta}{ds}\right]ds \tag{8}$$

These relations yield the net transverse force intensity, q, in terms of the displacement fleld variable, θ, the weight density w_0, the flexural rigidity and the seal tension, as shown in Eq. (9).

$$q = -EI\frac{d^3\theta}{ds^3} - w_0\cos\theta + T\frac{d\theta}{ds} \tag{9}$$

An estimation of the hydrostatic pressure acting on the seal for the selected displacement fleld is derived from a rear rangement of the terms in Eq. (2)

$$p_{hydro} = p_{cushion} - q \tag{10}$$

3.3 Model results

As an example condition we consider the configuration shown in Fig. 8. This seal shape was generated from the experimental conditions described in section 1.2.: forward speed 8 ft/sec, cushion pressure of 4.24 inches H_2O (0.153 psig) and 9.0 inches seal initial immersion depth with a total calculated hydrodynamic force of 124 lb acting on the seal. The upper left of the gure is the attachment point of the seal to the forward frame. Vessel travel is right to left. This configuration was gleaned from the photograph depicted in Fig. 4.

The angle of inclination as a function of arc length, $\theta = \theta(s)$, is then calculated from these data; 99 data points ({x, z} pairs) were derived from Fig 4. For smoothing purposes a 7^{th} order polynomial fit, based on least squares, was established. Differentiation of the polynomial then yields

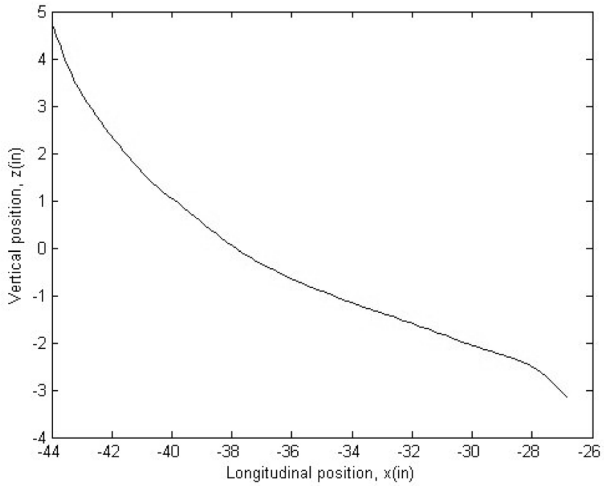

Fig. 8 Seal geometrical configuration example of a two-dimensional structural analysis

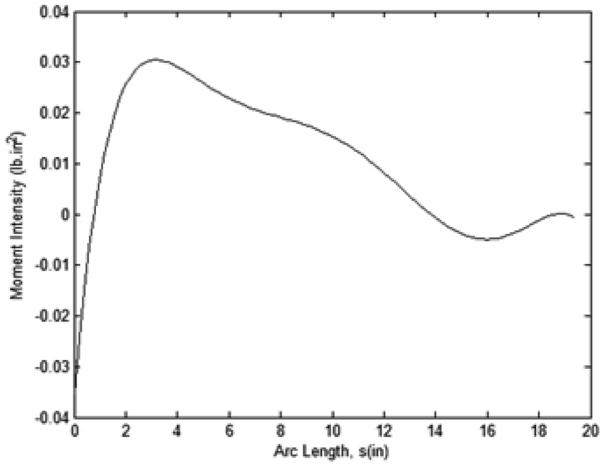

Fig. 9 Seal moment intensity determined from the example structural analysis

the moment intensity, determined from Eq. (5) and shown in Fig. 9. The flexural rigidity was determined to be approximately 0.4 lb-in^2 per unit width based on simple beam bending tests. It should be noted however that there is some variability of this value due to the presence of fibers within the polyurethane seal material. These fibers add considerable extensional stiffness within the plane of the seal. They are not however positioned at a precise location within the seal sheet thickness. The flexural rigidity does vary somewhat therefore as a function of position.

Using the approximated rigidity and the selected geometry the net pressure distribution can then be estimated. The hydrodynamic pressure determined from the above analysis is shown in Fig. 10.

Two curves are shown in Fig. 10. The lower curve shows the hydrodynamic pressure predicted considering only bending (and shear force) resistance of the seal caused by the difference in hydrodynamic and cushion pressures. However, the weight of the seal also contributes to the resistance of the seal. An additional factor is the seal tension which develops due to the nonlinear

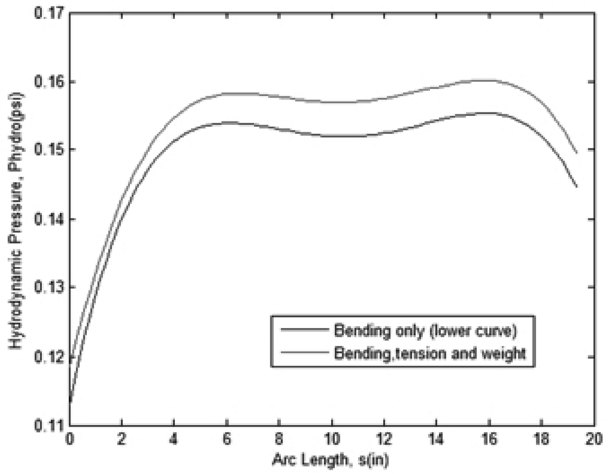

Fig. 10 Hydrodynamic pressures determined from the example structural analysis

geometric effects. Both of these additional effects are included with the bending resistance and shown in the upper curve of Fig. 10. Although these effects are evidently of secondary importance, they can be included without difficulty.

Note that the hydrodynamic pressure tends to decrease at the forward edge of the seal. This is a result of the slight negative curvature at that portion of the seal. This is for the most part believed to be an exception rather than the rule, as most portions of the seal has a positive curvature (bending upward) immediately after the connection to the frame. For the particular area selected as our example, our curvature in this region is negative, albeit for only a very short distance. We should also note the predicted pressures are very sensitive to the description of the angle of inclination since we are determining our pressures based on the third derivatives of this function.

It is also interesting to note that the tension in the seal affects the relation between deflection and pressure as much as indicated in Fig. 10. We note that the seal is completely free at the trailing edge, thereby keeping the tensile forces to a minimum. Some analyses treat the seal as a membrane when the ends of the structure are fixed; these allowing considerable tensile forces to build and resist transverse pressures; see for example (Doctors and McKesson 2006, Ulstein and Faltinsen 1998). Our conditions here however show that membrane forces are by no means sufficient and the bending resistance dominates. Thus the methods used for analyzing the structural response of the seal depend on the seals boundary conditions as well as the material and geometric arrangements.

4. Conclusions

A beam-bending theory approach to modeling the quasistatic condition of a two-dimensional SES vessel seal was demonstrated, based upon experimental conditions. The pressure fleld required to achieve the seal geometry for the given test conditions was derived from a beam-bending theory approach and independently form a CFD theory approach; the pressure fleld for these two approaches do not entirely agree. It is probable that in order to achieve convergence of the local pressure fleld that both disiplines, CFD and structural mechanics, will need to be considered

simultaneously in order to solve this fluid-structure interaction problem. It was also observed in the beam-bending analysis that the results were highly sensitive to local element inclination angle θ. The representative seal shape curve from the experimental quasistatic conditions used for analysis may not the the most appropriate way of defining the seal shape; apparently minor three-dimensional seal deformations may play a significant role in the total force on the seal. These modeling conditions will be investigated in future research.

Acknowledgments

The authors wish to acknowledge the continuing support of the US Office of Naval Research (ONR) through program manager Ms. Kelly Cooper, for the "Design Tools for the Sea-Base Connector Transformable-Craft (T-Craft) Prototype Demonstrator" research project, Award N00014-07-1-0856. This assistance has created many opportunities, including the encouragement of collaboration with a number of academic and industry researchers.

References

Bresch, P.K. (1976), "Motions of bow seal fingers in a surface effect ship flexible seal," David W. Taylor, Naval Ship Research and Development Center Report No. 76-0026.

Doctors, L.J. and McKesson, C.B. (2006), "The resistance components of a surface-effect ship", *Proceedings of the 26th Symposium on Naval Hydrodynamics*, Rome, Italy, September.

Graham, T.A., Sullivan, P.A. and Hinchey, M.J. (1985), "Skirt material effects on air cushion dynamic stability ", *J. Aircraft*, **22**(2), 101-108.

Graham, T.A. and Sullivan, P.A. (2002), "Pitch-heave dynamics of a segmented skirt air cushion", *J. Ship* Res., **46**(2), 121-137

Malakhoff, A. and Davis, S. (1981), "Dynamics of SES bow seal fingers", *Proceedings of the American Institute of Aeronautics and Astronautics Sixth Marine Systems Conference*, Seattle, Washington, September.

Sullivan, P.A., Charest, P.A. and MA, T. (1994), "Heave stiffness of an air cushion vehicle bag-and-finger skirt", *J. Ship Res.*, **38**(4), 302-307.

Ulstein, T. and O.D. Faltinsen (1998), "Cobblestone effect on SES", NATO Research and Technology Organisation", *Proceedings of the AVT Symposium on Fluid Dynamics Problems of Vehicles Operating near or in the Air-Sea Interface*, Amsterdam, The Netherlands, October .

Wilson, R.A., Wells, S.M. and Heber, C.E. (1979), "Powering predictions for surface effect ships based on model results", *J. Hydronautics*, **13**(4), 113-119.